

Fidelity, fidelity susceptibility and von Neumann entropy to characterize the phase diagram of an extended Harper model

Longyan Gong^{1,2,3*} and Peiqing Tong^{2,†}

¹*Department of Mathematics, Nanjing Normal University, Nanjing 210097, China*

²*Department of Physics, Nanjing Normal University, Nanjing 210097, China*

³*Center of Microfluidics Optics and Technology, Department of Mathematics and Physics, Nanjing University of Posts and Telecommunications, Nanjing 210003, China*

(Dated: today)

For an extended Harper model, the fidelity for two lowest band edge states corresponding to different model parameters, the fidelity susceptibility and the von Neumann entropy of the lowest band edge states, and the spectrum-averaged von Neumann entropy are studied numerically, respectively. The fidelity is near one when parameters are in the same phase or same phase boundary; otherwise it is close to zero. There are drastic changes in fidelity when one parameter is at phase boundaries. For fidelity susceptibility the finite scaling analysis performed, the critical exponents α , β , and ν depend on system sizes for the metal-metal phase transition, while not for the metal-insulator phase transition. For both phase transitions $\nu/\alpha \approx 2$. The von Neumann entropy is near one for the metallic phase, while small for the insulating phase. There are sharp changes in von Neumann entropy at phase boundaries. According to the variation of the fidelity, fidelity susceptibility, and von Neumann entropy with model parameters, the phase diagram, which including two metallic phases and one insulating phase separated by three critical lines with one bicritical point, can be completely characterized, respectively. These numerical results indicate that the three quantities are suited for revealing all the critical phenomena in the model.

PACS numbers: 71.30.+h, 03.67.Ud, 71.23.Ft

I. INTRODUCTION

In recent years, tools from the quantum-information theory^{1,2}, specifically the ground state fidelity³ and quantum entanglement^{4,5}, have been widely exploited to characterize quantum phase transitions(QPTs)⁶. For example, in one dimensional XY and Dicke model, fidelity between two ground states corresponding to slightly different values of the parameters drastically decreases at phase transition points³. Subsequently, similar properties are also found in fermionic^{7,8}, bosonic systems^{9,10} and other various spin systems^{11,12}. Very recently, fidelity susceptibility(FS) (the second derivative of fidelity) is introduced to signal QPTs in one-dimensional Hubbard models^{13,14,15}, the Lipkin-Meshkov-Glick model¹⁶, the Kitaev honeycomb model¹⁷, and various spin systems^{18,19,20}. It is found that FS is more curial than fidelity itself for it does not depend on the slightly difference values of model parameters. In Refs.^{21,22}, the fidelity between arbitrary two ground states is studied in one dimensional quantum Ising model. Singularities are found in fidelity surfaces for QPTs²². The main advantage of the fidelity to identify QPTs is that¹⁸, it need not a priori knowledge of the order parameter, topology, etc, since the fidelity is a purely Hilbert-space geometrical quantity.

At the same time, quantum entanglement has been extensively applied in condensed matter physics.^{23,24,25,26,27,28,29} For example, quantum entanglement measured by the von Neumann entropy has been studied in the Hubbard model for the dimer case²³, in the extended Hubbard model for different

band filling²⁴, in quantum small-world networks²⁵, and in low-dimensional semiconductor systems²⁶. It is found that the von Neumann entropy is suitable for analyzing the interplay between itinerant and localized features²³, as well as characterizing quantum phase transition^{24,27} and the localization-delocalization transition of electron states^{25,28,29}.

On the other hand, since the Hofstadter butterfly energy spectrum was found in 1976³⁰, the problem of electrons in two-dimensional periodic potential in a magnetic field has been attracted much attention^{31,32,33,34,35,36}. After fixing the quasimomentum in one of the directions, a one-dimensional quasiperiodic system called the Harper model is deduced³⁰. The system shows interesting metal-insulator transitions(MIT)^{32,33}. Considering the next-nearest-neighbor hopping for electron on the square lattice in a uniform magnetic field, an extended Harper model are proposed³⁴ and studied extensively³⁵. Very recently, a similar extended Harper model is introduced from two-dimensional electrons on the triangular lattice in a uniform magnetic field³⁶. The phase diagram has a very rich structure, which shown in Fig.1. In regions I and III the wave functions (spectra) are extended (absolutely continuous), and in the region II the wave functions are localized (pure points). On the three boundary lines, the wave functions (spectra) are critical (singular continuous). Besides the traditional MIT, there are novel transitions between the two metallic phases(MMT). At the bicritical point where the triangular lattice symmetry is retained, both level statistics and multifractal analysis show quantitatively different behaviors from those of other critical points³⁶.

Considering the above two aspects, we perform a de-

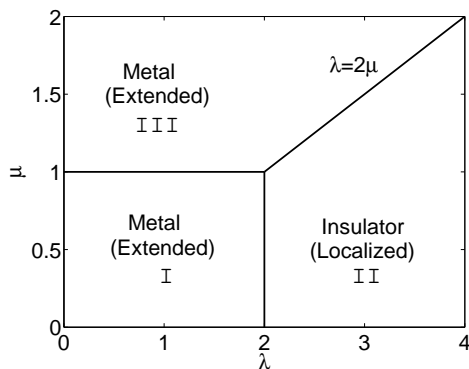


FIG. 1: Phase diagram of the extended Harper model.

tailed study of the fidelity between arbitrary two quantum states, FS and von Neumann entropy for the extended Harper model³⁶. For each of the three quantities, there are drastic changes at phase boundaries, i.e., the phase diagram can be distinguished according to the variations of them with model parameters. Our studies provide that the two tools, fidelity and von Neumann entropy, borrowed from the quantum-information theory, are well enough to identify phase transitions in the system.

The paper is organized as follows. In the next section the extended Harper model and the definitions of fidelity, FS and von Neumann entropy are introduced. In Sec. III the numerical results are presented. And we present our conclusions and discussions in Section IV.

II. THE EXTENDED HARPER MODEL, FIDELITY, FIDELITY SUSCEPTIBILITY AND VON NEUMANN ENTROPY

A. The extended Harper model

The tight-binding Hamiltonian for an electron moving on a triangular lattice in a magnetic field³⁶ can be reduced to

$$\begin{aligned}
 H = & - \sum_n [t_a + t_c e^{-2\pi i\phi(n-1/2)+ik_y}] c_n^\dagger c_{n-1} \\
 & - \sum_n [t_a + t_c e^{2\pi i\phi(n+1/2)-ik_y}] c_n^\dagger c_{n+1} \\
 & - 2 \sum_n t_b \cos(2\pi\phi n + k_y) c_n^\dagger c_n, \quad (1)
 \end{aligned}$$

where t_a , t_b and t_c are the hopping integral for each bond on the triangular lattice, ϕ is a flux that a uniform magnetic field penetrates each triangle, k_y is a momentum in the y direction, c_n^\dagger (c_n) is the creation (annihilation) operator of the n th site in the x direction.

Let $|n\rangle$ denote $|0, \dots, 1_n, \dots, 0\rangle$, the general eigenstate

of an electron with eigenenergy E_γ is

$$|\Psi_\gamma\rangle = \sum_n \psi_n^\gamma |n\rangle = \sum_n \psi_n^\gamma c_n^\dagger |0\rangle, \quad (2)$$

where ψ_n^γ is the amplitude of the γ th eigenstate at the n th site. If set $\lambda = 2\frac{t_b}{t_a}$, $\mu = \frac{t_c}{t_a}$ and t_a is taken as units, the eigenvalue equation³⁶ becomes

$$\begin{aligned}
 -[1 + \mu e^{-2\pi i\phi(n-1/2)+ik_y}] \psi_{n-1} - [1 + \mu e^{2\pi i\phi(n+1/2)-ik_y}] \\
 \psi_{n+1} - \lambda \cos(2\pi\phi n + k_y) \psi_n = E \psi_n. \quad (3)
 \end{aligned}$$

At $\mu = 0$ and ϕ is irrational, this is reduced to the Harper equation. Intensively analytical and numerical studies^{32,33} for the Harper model show that for $\lambda > 2$ the spectrum is pure-point like and all eigenstates are exponentially localized. For $\lambda < 2$ the spectrum becomes continuous with delocalized eigenstates corresponding to ballistic classical motion. For $\lambda = 2$ the situation is critical with a singular-continuous multifractal spectrum and power law localized eigenstates. MIT can occur at $\lambda = 2$.

B. Fidelity

Let $|\Psi_0(\lambda, \mu)\rangle$ denote the lowest band edge state. According to the definition of fidelity^{1,3,21,22}, the quantum fidelity (or the modulus of the overlap of eigenstates) is given by

$$F(\lambda, \mu; \lambda_0, \mu_0) = |\langle \Psi_0(\lambda, \mu) | \Psi_0(\lambda_0, \mu_0) \rangle|. \quad (4)$$

Obviously, $F = 1$ if $\lambda = \lambda_0$ and $\mu = \mu_0$.

C. Fidelity susceptibility

Similarly as that shown in Ref.³, the fidelity for two lowest edge states with a slightly different parameter values is defined as

$$F(q) = |\langle \Psi_0(q) | \Psi_0(q + \delta q) \rangle|. \quad (5)$$

For simplicity, a certain path $q = q(\lambda, \mu)$ in parameter spaces can always be supposed. Then the FS can be calculated as^{13,17,37}

$$\chi^F = \lim_{\delta q \rightarrow 0} \frac{-2 \ln F(q)}{\delta q^2} = \sum_{a=\lambda, \mu; b=\lambda, \mu} g_{a,b} n^a n^b, \quad (6)$$

where $n^\lambda = \partial q / \partial \lambda$ ($n^\mu = \partial q / \partial \mu$) denotes the tangent units vector at the give parameter point (λ, μ) . For the present model, let define the driving Hamiltonians

$$H_\lambda = - \sum_n \cos(2\pi\phi n + k_y) c_n^\dagger c_n \quad (7)$$

and

$$\begin{aligned}
 H_\mu = & - \sum_n [e^{-2\pi i\phi(n-1/2)+ik_y}] c_n^\dagger c_{n-1} \\
 & - \sum_n [e^{2\pi i\phi(n+1/2)-ik_y}] c_n^\dagger c_{n+1}. \quad (8)
 \end{aligned}$$

We have

$$g_{ab} = \sum_{\gamma \neq 0} \frac{\langle \Psi_\gamma(q) | H_a | \Psi_0(q) \rangle \langle \Psi_0(q) | H_b | \Psi_\gamma(q) \rangle}{(E_\gamma - E_0)^2}. \quad (9)$$

D. von Neumann entropy

The general definition of entanglement is based on the von Neumann entropy³⁸. For an electron in the system, there are two local states at each site, i.e., $|0\rangle_n, |1\rangle_n$. The local density matrix ρ_n is defined^{23,24,25,29} by

$$\rho_n = z_n |1\rangle_{nn} \langle 1| + (1 - z_n) |0\rangle_{nn} \langle 0|, \quad (10)$$

where $z_n = \langle \Psi_\gamma | c_n^\dagger c_n | \Psi_\gamma \rangle = |\psi_n^\gamma|^2$ is the local occupation number at the n th site. Consequently, the corresponding von Neumann entropy related to the n th site is

$$E_{vn}^\gamma = -z_n \log_2 z_n - (1 - z_n) \log_2 (1 - z_n). \quad (11)$$

For nonuniform systems, the value of E_{vn}^γ depends on the site position n . At an eigenstate $|\Psi_\gamma\rangle$, we define a site-averaged von Neumann entropy

$$E_v^\gamma = \frac{1}{N} \sum_{n=1}^N E_{vn}^\gamma, \quad (12)$$

where N is the system size. From the definition (12), it shows that for an extended state that $\psi_n^\gamma = \frac{1}{\sqrt{N}}$ for all n , $E_v^\gamma = -\frac{1}{N} \log_2 \frac{1}{N} - (1 - \frac{1}{N}) \log_2 (1 - \frac{1}{N}) \approx \frac{1}{N} \log_2 N$ at $N \rightarrow \infty$, and for a localized state that $\psi_n^\gamma = \delta_{nn^\circ}$ (n° is a given site), $E_v^\gamma = 0$. In the paper all the values of E_v^γ and E_{vn}^γ are scaled by $\frac{1}{N} \log_2 N$. From the two examples, we know the scaled E_v^γ is near 1 when eigenstates are extended, and near zero when eigenstates are localized. Henceforth, we omit “scaled” for simplicity.

In order to analyze the influence of system parameters on the von Neumann entropy for all the eigenstates, we define a spectrum-averaged von Neumann entropy as a further gross measure, i.e.,

$$\langle E_v \rangle = \frac{1}{M} \sum_{\gamma} E_v^\gamma, \quad (13)$$

where M is the number of all the eigenstates.

III. NUMERICAL RESULTS

In numerical calculations, without loss of generality, we set $k_y = 0$. As a typical case, $\phi = (\sqrt{5} - 1)/2$. In fact as is customary in the context of quasiperiodic system, the value of ϕ may be approximated by the ratio of successive Fibonacci numbers— $F_m = F_{m-2} + F_{m-1}$ with $F_0 = F_1 = 1$. In this way, choosing $\phi = F_{m-1}/F_m$ and system size $N = F_m$, we can obtain the periodic approximant for the quasiperiodic potential. We directly diagonalize the eigenvalue Eq.(2) at different values (λ, μ) and

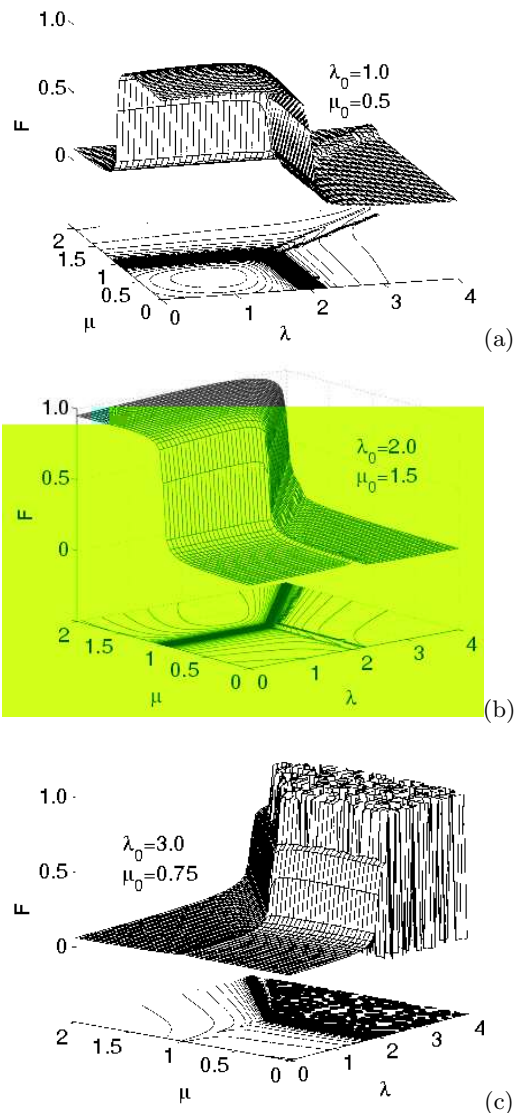


FIG. 2: The fidelity $F(\lambda, \mu; \lambda_0, \mu_0)$ and its contour map as functions of (λ, μ) at (a), (b) and (c) for $(\lambda_0, \mu_0) = (1.0, 0.5)$, $(2.0, 1.5)$ and $(3.0, 0.75)$, which corresponding to the system in the metal phase I, the metal phase III, and the insulator phase II, respectively.

get all the eigenvalues E_γ and the corresponding eigenstates $|\Psi_\gamma\rangle$. From the formulas (4–13), we can obtain the fidelity $F(\lambda, \mu; \lambda_0, \mu_0)$, the FS χ_F , the site-averaged von Neumann entropy E_v^γ and the spectrum-averaged von Neumann entropy $\langle E_v \rangle$, respectively. Henceforth, for simplicity we denote F to $F(\lambda, \mu; \lambda_0, \mu_0)$. In all the figures the system sizes N is chosen to Fibonacci number 987 unless specially stated.

A. Fidelity

In the metallic phase I, metallic phase III, and insulating phase II, we choose $(\lambda_0, \mu_0) = (1.0, 0.5)$, $(2.0, 1.5)$ and

(3.0, 0.75) as examples, respectively. The corresponding fidelity F varying with parameters λ and μ are shown in Fig.2. At the same time, the contour maps of the fidelity are also shown. It shows that when parameters are at the same phase, the fidelity is near one; otherwise, the fidelity is very small. It is interesting that, though the phase I and III are both metallic phases and the corresponding wave functions are all extended, the fidelity is small when parameters are in the two phases respectively. This can be understood from the corresponding “classical orbits” Hamiltonian³⁶: for Phase I, the contour lines of the Hamiltonian are extended in x direction but localization in the y direction, while for Phase III, the contour lines are extended in $x + y$ direction but localized in the $x - y$ direction. Therefore, the two phases are different. At the same time, these contour maps divide the parameter space to different regions, which is good agreement with the phase diagram shown in Fig.1. Comparing with the fidelity shown in Fig.2(a) and (b), the fidelity in Fig.2(c) changes drastically with model parameters. It is because the band edge states in the insulating phase II may be localized in different regions of space and the overlap of these states may be large or small.

At the three phase boundaries, we choose $(\lambda_0, \mu_0) = (1.0, 1.0)$, $(2.0, 0.5)$ and $(3.0, 1.5)$ as examples, which corresponding to the system at the boundaries between Phase I and III, Phase I and II and Phase III and II, respectively. The fidelity F varying with λ and μ are shown in Fig.3. It shows that when parameters (λ, μ) and (λ_0, μ_0) are at a same critical line, the fidelity is near one; otherwise, the fidelity is relatively small. It is interesting that if a point (λ_0, μ_0) in the critical line between Phase I and II (Phase I and II, Phase II and III), the fidelity in the both phases is relatively large. Similar to that shown in Fig.2, these contour maps of fidelity also divide the parameter space to three regions, which is same as the phase diagram shown in Fig.1.

At the bicritical point $(\lambda_0, \mu_0) = (2.0, 1.0)$, the fidelity F and its contour map as functions of λ and μ are plotted in Fig.4. It shows that when $(\lambda, \mu) = (2.0, 1.0)$, F is maximal and equal to one, when (λ, μ) for the three critical lines, F becomes relatively small, and when (λ, μ) in Phase I, II and III, F becomes relatively smaller. All these certify that the bicritical point itself is different from others points, which is agreement with the conclusion that the bicritical point is a particular critical point as investigated in Ref.³⁶. At the same time, the contour of fidelity can reflect the phase diagram shown in Fig.1.

B. Fidelity Susceptibility

According to the definition of FS in Eq.(6), its values depend on g_{ab} and a specific direction of parameter path $q = q(\lambda, \mu)$ ¹⁷. The tangent unit vector (n^λ, n^μ) which defines the direction may be different, though g_{ab} does not depend on parameter paths. In the following, the FS for $(n^\lambda, n^\mu) = (0, 1)$, $(1, 0)$, and $(1/\sqrt{5}, -2/\sqrt{5})$ are

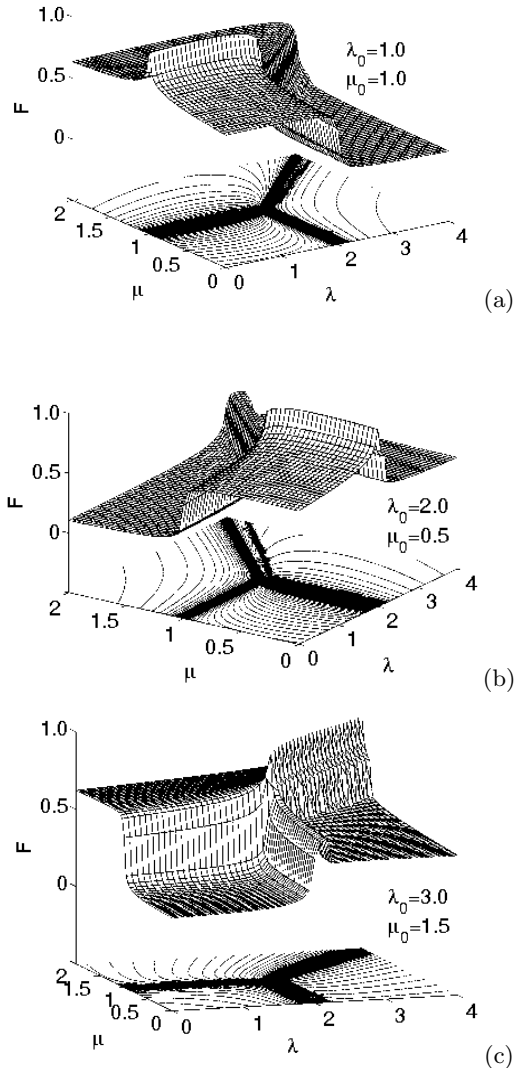


FIG. 3: The fidelity $F(\lambda, \mu; \lambda_0, \mu_0)$ and its contour map as functions of (λ, μ) at (a), (b) and (c) for $(\lambda_0, \mu_0) = (1.0, 1.0)$, $(2.0, 0.5)$ and $(3.0, 1.5)$, which corresponding to the system at the phase boundaries between I and III, I and II, and III and II, respectively.

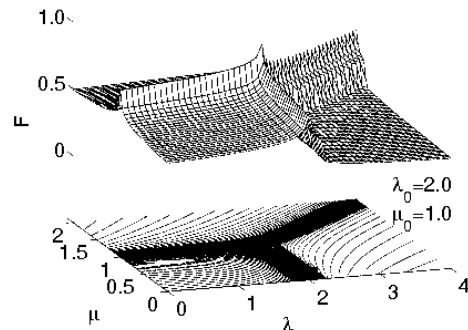


FIG. 4: The fidelity $F(\lambda, \mu; \lambda_0, \mu_0)$ and its contour map as functions of (λ, μ) for $(\lambda_0, \mu_0) = (2.0, 1.0)$, which corresponding to the system at the bicritical point.

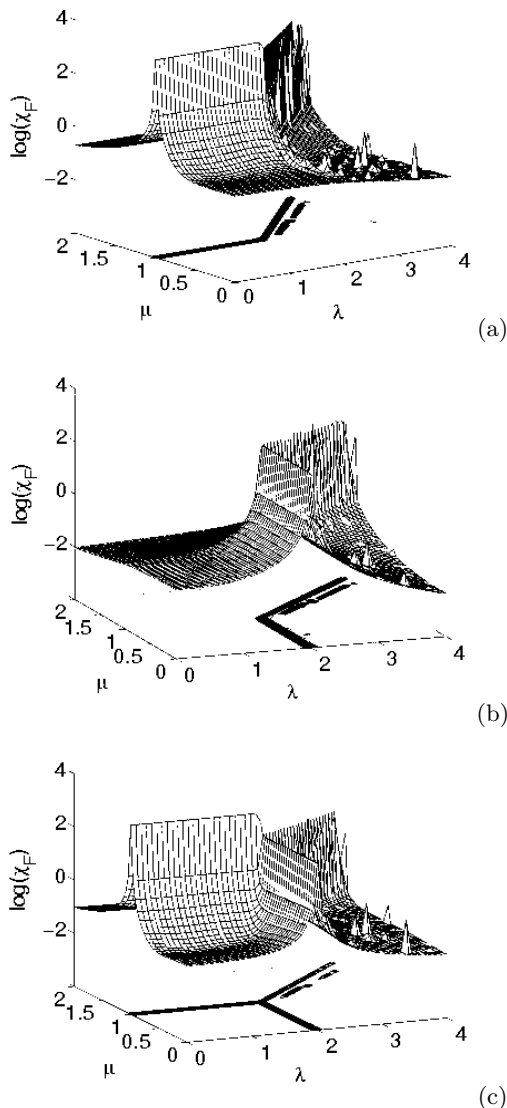


FIG. 5: The logarithmic plots of fidelity susceptibility χ_F and its contour maps as functions of (λ, μ) from different parameter paths $q = q(\lambda, \mu)$. The tangent units vector (n^λ, n^μ) of paths equals to (a)(0, 1), (b)(1, 0), (c)(1/ $\sqrt{5}$, -2/ $\sqrt{5}$), respectively.

shown in Fig.5(a), (b) and (c), respectively, which are corresponding to that only μ , only λ changes and both change simultaneily.

Fig.5 shows the $\chi_F(\lambda, \mu)$ are different when choosing different parameter paths. For Fig.5(a), only the driving Hamiltonian H_μ effects the values of χ_F . From the corresponding contour maps, the boundaries between the metallic phase III and other two phases are identified, i.e., there are sharp changes in χ_F at these phase boundaries, while for Fig.5(b), only H_λ effects χ_F and the boundaries between the insulating phase II and other two phases are identified. The combination of the two contour maps in Fig.5(a) and (b) is consistence with the phase diagram

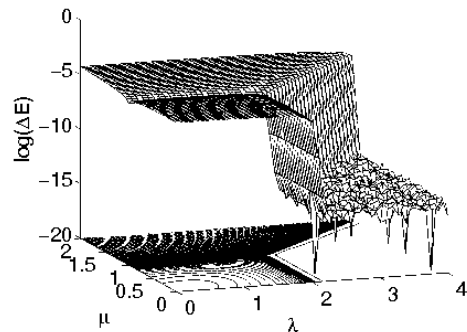


FIG. 6: $\log(\Delta E)$ varying with (λ, μ) , here ΔE is the gap between E_1 and E_0 at (λ, μ) .

that shown in Fig.1. For Fig.5(c), both H_λ and H_μ effect χ_F and the corresponding contour maps itself can reflect the phase diagram. In Fig.5(a), (b) and (c), the varying of χ_F in the insulating phase II is not smooth, which is due to the gap between E_0 and E_γ may be close to zero at some parameters(see Eq.9). For this, the logarithmic plots of the gap ΔE for the first excited state eigenenergy E_1 and ground state eigenenergy E_0 varying with (λ, μ) are shown in Fig.6. One sees that in Phase II, all the values of ΔE are very small and some almost are equal to zeros, therefore the fidelity F changes sharply at these parameter points. It is interesting that the contour maps of ΔE divide the parameter space to three regions, which is also consistence with the phase diagram shown in Fig.1.

In order to study the critical behavior around critical points (λ_c, μ_c) , we study the finite scaling analysis of FS^{13,15,16,17} and obtain the corresponding critical exponents. It has been found that these critical exponents and different scaling behaviors of FS can characterize the universality classes of phase transitions¹⁵. Firstly, we study the transition between the metallic phase I and metallic phase III and choose the critical point $(\lambda_c = 1.0, \mu_c = 1.0)$ as an example. Near the critical parameter with the tangent units vector $(n^\lambda = 0, n^\mu = 1)$ of parameter paths, the χ_F is calculated for various system sizes N , which corresponding to the case that shown in Fig.6(a). Along the parameter path, the FS reaches its maximum value χ_{Fmax} at a certain position μ_{max} . The scaling behaviors of χ_{Fmax} and $\mu_{Fmax} - \mu_c$ are given in Fig.7(a) and (b), respectively, which shows that $\chi_{Fmax} \propto N^\alpha$ and $\mu_{Fmax} - \mu_c \propto N^\beta$. All $\beta < 0$, which means μ_{Fmax} tends to the critical point μ_c in the thermodynamic limit. For the system sizes N are chosen to the Fibonacci number F_m with $m = 3l + 1$ and $m \neq 3l + 1$ for integer l , the system sizes are divided to two cases³⁶. It is found that $\alpha \approx 2.0$ and $\beta \approx -2.0$ for $m \neq 3l + 1$, while $\alpha = 4.9371$ and $\beta = -1.5022$ for $m = 3l + 1$. In Fig.8, the corresponding scaling functions are plotted. It shows that the exponent $\nu \approx 1.0$ for $m \neq 3l + 1$, while $\nu = 2.4718$ for $m = 3l + 1$. Although $\alpha(\beta)$ are different for $m = 3l + 1$ and $m \neq 3l + 1$, the scaling relation $\alpha/\nu \approx 2$ is universal.

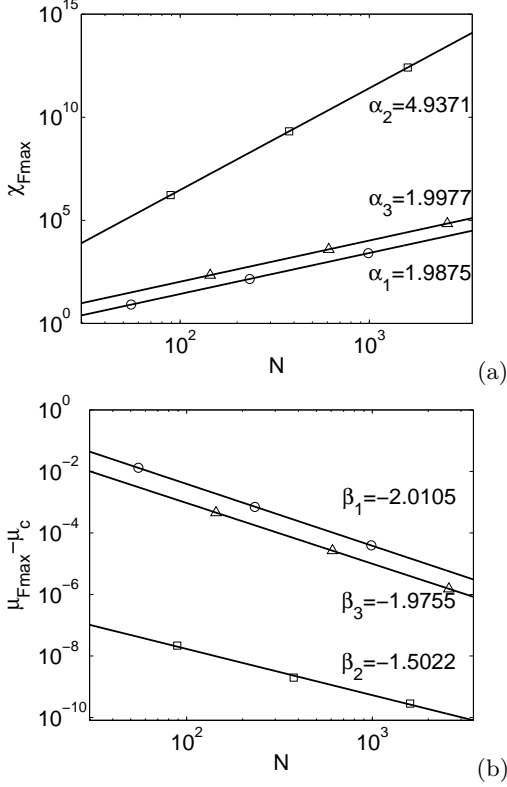


FIG. 7: The scaling behaviors of (a) χ_{Fmax} and (b) $\mu_{Fmax} - \mu_c$, respectively. The system sizes $F_{3l} = 55, 233, 987$ (\circ), $F_{3l+1} = 89, 377, 1597$ (\square) and $F_{3l+2} = 144, 610, 2584$ (\triangle), respectively. At the same time, the corresponding fitted lines are also shown, respectively.

The scaling relation is same as that for a one-dimensional asymmetric Hubbard model studied by Gu *et al*¹⁵.

To understand the different behaviors between the systems with $N = F_{3l+1}$ and $N \neq F_{3l+1}$, we analyse carefully the structure of the system. According to Fibonacci numbers $F_m = F_{m-2} + F_{m-1}$ with $F_0 = F_1 = 1$, F_{3l} and F_{3l+1} are odd, which can be written as $2k_1 + 1$ and $2k_2 + 1$ with integers k_1 and k_2 , respectively. For $N = F_{3l+1}$, $\phi = \frac{F_{3l}}{F_{3l+1}} = \frac{2k_1+1}{2k_2+1}$ and $\mu = 1$, the hopping term of Eq.(3), $-[1 + \mu e^{2\pi i \phi(n+1/2)}] = -[1 + e^{2\pi i \frac{2k_1+1}{2k_2+1} \frac{2n+1}{2}}] = 0$ at the site $n = k_2$, i.e., a bond between k_2 and $(k_2 + 1)$ th site breaks. The system is divided to two segments. For $N \neq F_{3l+1}$, it does not happen. This induces differences between the energy spectrum of $N = F_{3l+1}$ and $N \neq F_{3l+1}$ ³⁶.

Secondly, we study the transition between the metallic phase I and insulating phase II and choose the critical parameter ($\lambda_c = 2.0, \mu_c = 0.5$) as an example. Near the critical parameter with the tangent units vector ($n^\lambda = 1, n^\mu = 0$), the FS χ_F is calculated for various system sizes N , which corresponding the case shown in Fig.6(b). From Figs. 9 and 10, it is found that for all system sizes, 55, 89, ..., 2584, the exponents α, β and ν are same and

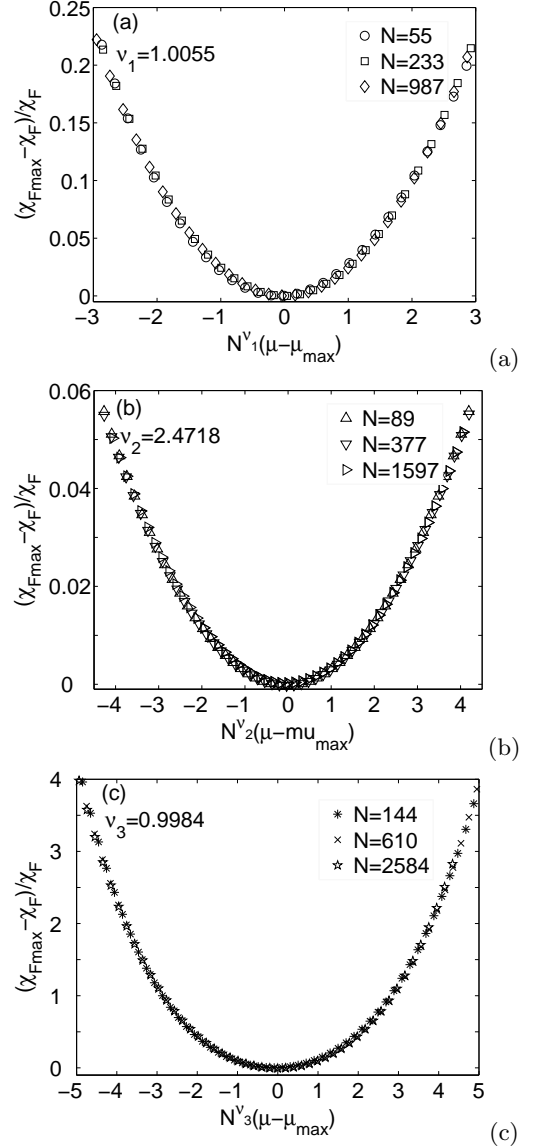


FIG. 8: The finite size scaling analysis is performed for $(\chi_{Fmax} - \chi_F)/\chi_F$ as a function $N^\nu(\mu - \mu_{max})$.

the the scaling relation $\alpha/\nu \approx 2$ is also obtained. We have studied the transition between the metallic phase III and insulating phase II, the results are similar and the relation $\alpha/\nu \approx 2$ is also tenable.

C. von Neumann entropy

The von Neumann entropy has been found to be a suitable quantity to characterize the localization properties of electronic states^{25,28,29}. Fig.11(a) and (b) show the site-averaged von Neumann entropy E_v^γ for the lowest edge states and the spectrum-averaged von Neumann entropy $\langle E_v \rangle$, respectively. The varyings of the two quantities with parameters (λ, μ) are similar. $E_v^\gamma(\langle E_v \rangle)$ is near

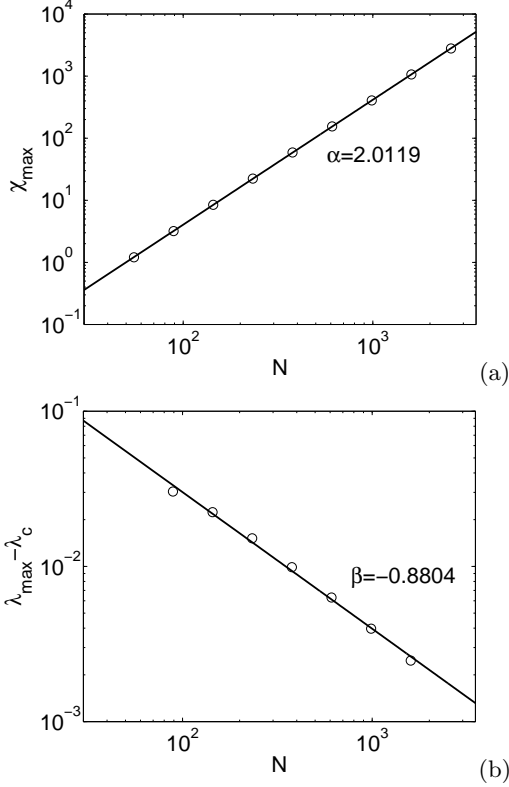


FIG. 9: The scaling behaviors of (a) χ_{Fmax} and (b) $\lambda_{Fmax} - \lambda_c$, respectively. The system sizes are 55, 89, ..., 2584.

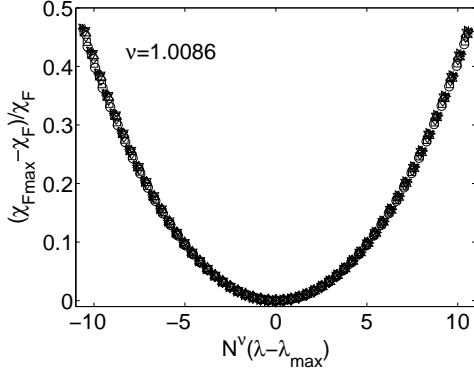


FIG. 10: The finite size scaling analysis is performed for $(\chi_{Fmax} - \chi_F) / \chi_F$ as a function $N^\nu (\lambda - \lambda_{max})$ for the system sizes are 55, 89, ..., 2584.

1 in the metallic phase I and III and relatively small in the insulating phase II. There are sharp decreases in E_v^γ ($\langle E_v \rangle$) at phase boundaries. The contour maps of them divide the parameter space to three parts, which is consistent with the phase diagram shown in Fig.1.

Conventionally, the inverse participation ratio (IPR) is often used as a measure of the wave-functions localization length³⁹. The larger is the IPR, the more delocalized the eigenstate is. It has found that the

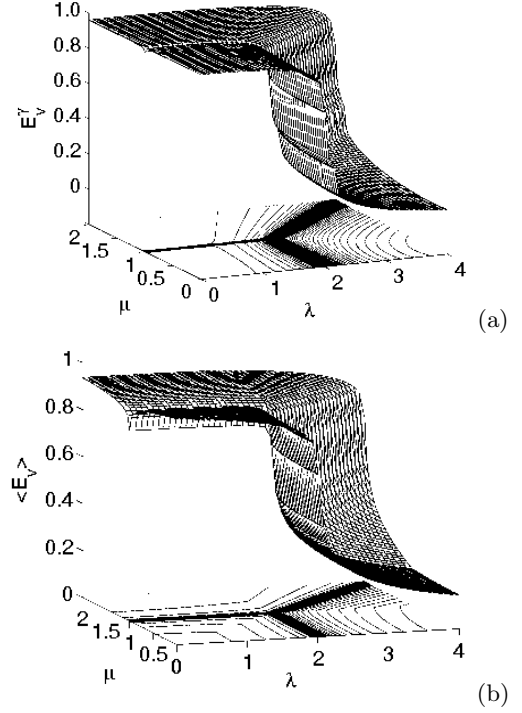


FIG. 11: The site-averaged von Neumann entropy E_v^γ for the lowest edge states (a) and the spectrum-averaged von Neumann entropy $\langle E_v \rangle$ (b) as functions of (λ, μ) , respectively.

site-averaged von Neumann entropy E_v^γ increases exponentially with the IPR²⁹, i.e., E_v^γ can reflect the localization properties of electronic states. Fig.12(a)-(d) show E_v^γ varying with eigenenergy E_γ for $(\lambda, \mu) = (1.0, 0.5)$, $(3.0, 0.75)$, $(1.0, 1.0)$ and $(2.0, 0.5)$, which corresponding to the metallic phase, the insulating phase, the MMT and the MIT, respectively. In Fig.12(a), almost all the E_v^γ are near 1, which means these states are delocalized. Comparing Fig.12(b) with Fig.12(a), all the E_v^γ are small, which means that all eigenstates are localized. In Fig.12(c) and (d), there coexist large, middle, and small E_v^γ , which means the eigenstates are critical. Though all eigenstates for the three phase boundaries and the bicritical point are critical, the values of the spectrum-averaged von Neumann entropy $\langle E_v \rangle$ are different. Comparing to each other, the $\langle E_v \rangle$ for boundaries between the metallic phase I and III are large, for the bicritical point are middle, and for boundaries between metallic phase and insulator are small, which can be seen from Fig.11(b). All these indicate that, judging from the varying of von Neumann entropy with parameter (λ, μ) , the phase diagram can be completely characterized.

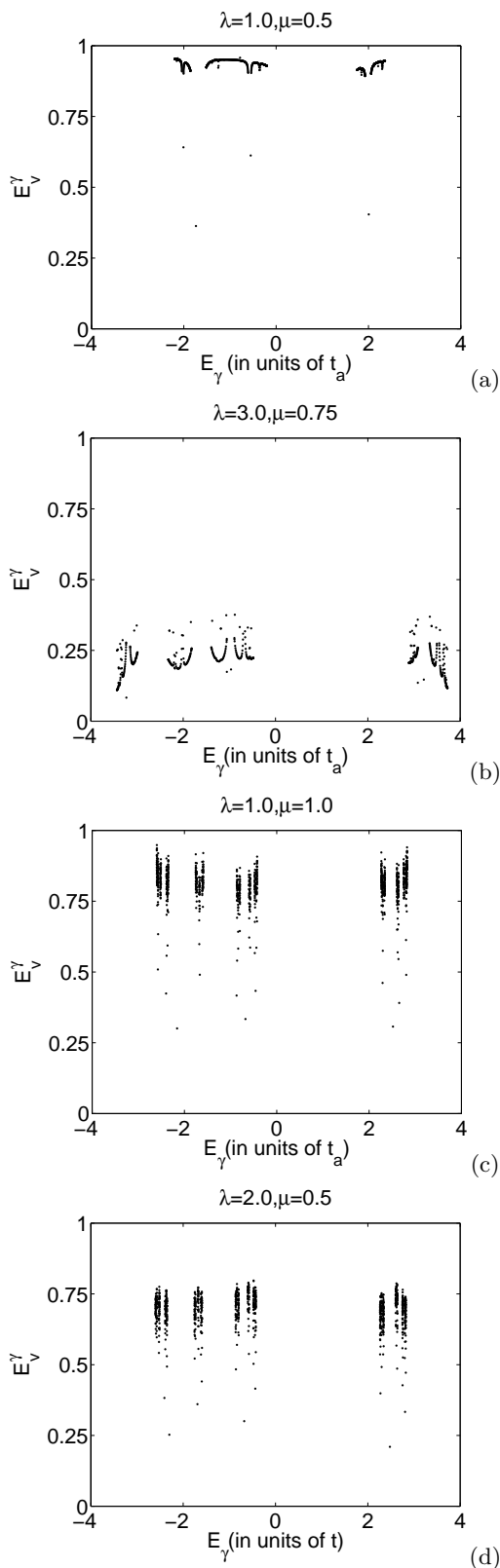


FIG. 12: The site-averaged von Neumann entropy E_v^γ varying with eigenenergy E_γ at $(\lambda, \mu) = (1.0, 0.5)$, $(3.0, 0.75)$, $(1.0, 1.0)$ and $(2.0, 1.0)$ for (a), (b), (c) and (d), respectively.

IV. CONCLUSIONS AND DISCUSSIONS

For the extended Harper model introduced in Ref.³⁶, we have studied the fidelity between two lowest band edge states corresponding to different model parameters, the FS and the von Neumann entropy of the lowest band edge states, and the spectrum-averaged von Neumann entropy. All the three quantities can well characterize the rich phase diagram of the interesting model.

In detail, firstly, the fidelity varying with parameters (λ, μ) for seven groups of fixing values (λ_0, μ_0) is studied, which corresponding to different phases, different phase boundaries and the bicritical point. When parameters are in the same phase or same boundary, the fidelity is near one, otherwise, it is small. There are drastic changes in fidelity when one parameter corresponding to phase boundaries. At the same time, the contour maps of fidelity divide the parameter space to three regions, which is a good agreement with the phase diagram of the model. In fact, these conclusions are valid for arbitrary fixing values (λ_0, μ_0) in the parameter space. It indicates that the fidelity can well reflect the different phases and reveal different phase transitions.

Secondly, the FS is studied and the finite scaling analysis is performed for the MMT and the MIT. The contour maps of FS can well reflect the phase diagram. At the MMT, the critical exponents $\alpha(\beta, \nu)$ for system sizes $F_{m=3l+1}$ and $F_{m \neq 3l+1}$ are different, but the relation that $\nu/\alpha \approx 2$ is universal. At the MIT, the critical exponents for all system sizes are same and the relation that $\nu/\alpha \approx 2$ is also tenable.

At last, the von Neumann entropy is studied. It is near one in the metallic phase, while small in the insulating phase. There are sharp changes at phase boundaries. There are difference in the values of spectrum-average von Neumann entropy for the three phase boundaries and the bicritical point. The contour maps of von Neumann entropy is consistence with the phase diagram. All these indicate that the different phases and phase transitions can be completely distinguished by von Neumann entropy.

Acknowledgments

Project supported by the National Nature Science Foundation of China (Grant Nos 90203009 and 10674072), by the Specialized Research Fund for the Doctoral Program of Higher Education (Grant No 20060319007), by the Excellent Young Teacher Program of the Ministry of Education of China.

-
- * Email address:lygong@njupt.edu.cn.
† Corresponding author. Email address:pqtong@njnu.edu.cn.
- ¹ M. A. Nielsen and I. L. Chuang, *Quantum Computation and Quantum Information* (Cambridge University Press, 2000, Cambridge).
 - ² See, for example, *The Physics of Quantum Information*, edited by D. Bouwmeester, A. Ekert, and A. Zeilinger (Springer, Berlin, 2000).
 - ³ P. Zanardi and N. Paunkovic, *Phys. Rev. E* **74**, 031123(2006).
 - ⁴ T. J. Osborne and M. A. Nielsen, *Phys. Rev. A* **66**, 32110 (2002).
 - ⁵ A. Osterloh, L. Amico, G. Falci, and R. Fazio, *Nature* **416**, 608 (2002).
 - ⁶ S. Sachdev, *Quantum Phase Transitions* (Cambridge University Press, 1999, Cambridge).
 - ⁷ M. Cozzini, P. Giorda, and P. Zanardi, *Phys. Rev. B* **75**, 014439(2007).
 - ⁸ N. Paunković and V. R. Vieira, *Phys. Rev. E* **77**, 011129(2008).
 - ⁹ P. Buonsante and A. Vezzani, *Phys. Rev. Lett.* **98**, 110601 (2007).
 - ¹⁰ N. Oelkers and J. Links, *Phys. Rev. B* **75**, 115119 (2007).
 - ¹¹ S. Chen, L. Wang, S. J. Gu, and Y. Wang, *Phys. Rev. E* **76**, 061108 (2007).
 - ¹² P. Zanardi, H. T. Quan, X. G. Wang and C. P. Sun, *Phys. Rev. A* **75**, 032109 (2007).
 - ¹³ W. L. You, Y. W. Li and S. J. Gu, *Phys. Rev. E* **76**, 022101 (2007).
 - ¹⁴ L. Campos Venuti, M. Cozzini, P. Buonsante, F. Massel, N. Bray-Ali and P. Zanardi, arXiv:0801.2473.
 - ¹⁵ S. J. Gu, Ho Man Kwok, W. Q. Ning, and H. Q. Lin, *Phys. Rev. B* **77**, 245109 (2008).
 - ¹⁶ H.M. Kwok, W.Q. Ning, S. J. Gu, H. Q. Lin, arXiv:0710.2581.
 - ¹⁷ S. Yang, S. J. Gu, C. P. Sun and H. Q. Lin, *Phys. Rev. A* **78**012304(2008).
 - ¹⁸ M. T. Yang, *Rev. B* **76**, 180403(R)(2007).
 - ¹⁹ Y.-C. Tzeng and M. F. Yang, *Phys. Rev. A* **77**, 012311 (2008).
 - ²⁰ S. Chen, L. Wang, Y. J. Hao, and Y. P Wang, *Phys. Rev. A* **77**, 032111 (2008).
 - ²¹ H. Q. Zhou, J. H. Zhao, and B. Li, arXiv:0704.2940.
 - ²² H. Q. Zhou, J. H. Zhao, H. L. Wang and B. Li, arXiv:0711.4651.
 - ²³ P. Zanardi, *Phys. Rev. A* **65**, 042101(2002).
 - ²⁴ S. J. Gu, S. S. Deng, Y. Q. Li, and H. Q. Lin, *Phys. Rev. Lett.* **93**, 086402 (2004).
 - ²⁵ L. Y. Gong and P. Q. Tong, *Phys. Rev. E* **74**, 056103 (2006).
 - ²⁶ F. Buscemi, P. Bordone, and A. Bertoni, *phys. Rev. A* **73**, 052312 (2006).
 - ²⁷ D. Larsson and H. Johannesson, *Phys. Rev. A* **73**, 042320 (2006).
 - ²⁸ L. Y. Gong and P. Q. Tong, *Phys. Rev. A* **71**, 042333 (2005).
 - ²⁹ L. Y. Gong and P. Q. Tong, *Phys. Rev. B* **76**, 085121 (2007).
 - ³⁰ D. R. Hofstadter, *Phys. Rev. B* **14**, 2239 (1976).
 - ³¹ F. H. Claro and G. H. Wannier, *Phys. Rev. B* **19**, 6068 (1979).
 - ³² S. Aubry and G. Andre, *Ann. Israel Phys. Soc.* **3**, 133 (1980).
 - ³³ J. B. Sokoloff, *Phys. Rep.* **126**, 189 (1985).
 - ³⁴ J. H. Han, D. J. Thouless, H. Hiramoto, and M. Kohmoto, *Phys. Rev. B* **50**, 11365 (1994).
 - ³⁵ Y. Takada, K. Ino and M. Yamanaka, *Phys. Rev. E* **70**, 066203 (2004).
 - ³⁶ K. Ino and M. Kohmoto, *Phys. Rev. B* **73**, 205111 (2006).
 - ³⁷ P. Zanardi, P. Giorda, and M. Cozzini, *Phys. Rev. Lett.* **99**, 100603 (2007).
 - ³⁸ C. H. Bennett, H. J. Bernstein, S. Popescu, and B. Schumacher, *Phys. Rev. A*, **53** 2046(1996).
 - ³⁹ B.Kramer and A. MacKinnon, *Rep. Prog. Phys.* **56** 1469 (1993).